Article

Machine Learning-Inspired Hybrid Precoding for HAP Massive MIMO Systems with Limited RF Chains

Shabih ul Hassan [1], Talha Mir [2], Sultan Alamri [3,*], Naseer Ahmed Khan [4] and Usama Mir [5]

1   Information and Communication, University of Science and Technology of China, Hefei 230052, China
2   Department of Electronic Engineering, Baluchistan University of IT, Engineering and Management Sciences Pakistan (BUITEMS), Quetta 87300, Pakistan
3   College of Computing and Informatics, Saudi Electronic University, Riyadh 13316, Saudi Arabia
4   School of Computer Science, Northwestern Polytechnical University, Xi'an 710060, China
5   School of Computer Science, University of Windsor, Windsor, ON N9B 3P4, Canada
*   Correspondence: salamri@seu.edu.sa

Abstract: Energy efficiency (EE) is the main target of wireless communication nowadays. In this paper, we investigate hybrid precoding (HP) and massive multiple-input multiple-output (MIMO) systems for a high-altitude platform (HAP). The HAP is an emerging solution operating in the stratosphere at an amplitude of up to 20–40 km to provide communication facilities that can achieve the best features of both terrestrial and satellite systems. The existing hybrid beamforming solution on a HAP requires a large number of high-resolution phase shifters (PSs) to realize analog beamforming and radio frequency (RF) chains associated with each antenna and achieve better performance. This leads to enormous power consumption, high costs, and high hardware complexity. To address such issues, one possible solution that has to be tweaked is to minimize the number of PSs and RFs or reduce their power consumption. This study proposes an HP sub-connected low-resolution bit PSs to address these challenges while lowering overall power consumption and achieving EE. To significantly reduce the RF chain in a massive MIMO system, HP is a suitable solution. This study further examined adaptive cross-entropy (ACE), a machine learning-based optimization that optimizes the achievable sum rate and energy efficiency in the Rician fading channel for HAP massive MIMO systems. ACE randomly generates several candidate solutions according to the probability distribution (PD) of the elements in HP. According to their sum rate, it adaptively weights these candidates' HP and improves the PD in HP systems by minimizing the cross-entropy. Furthermore, this work suggests energy consumption analysis performance evaluation to unveil the fact that the proposed technique based on a sub-connected low-bit PS architecture can achieve near-optimum EE and sum rates compared with the previously reported methods.

Keywords: energy efficiency; hybrid precoding; massive MIMO; machine learning; adaptive cross-entropy; Rician fading channel; HAP

1. Introduction

The capacity demand in fifth-generation (5G) wireless communication and beyond is facing major challenges, particularly in terms of "last mile" transmission. Line-of-sight (LOS) propagation paths are a bottleneck on the ground unless a significant number of base stations (BS) are deployed, while satellite systems have capacity limitations. To effectively provide high data rates, massive numbers of antennas, and consistent coverage, innovative technologies are required [1,2]. The high-altitude platform (HAP) is an emerging solution, operating at an amplitude of up to 20–40 km to provide communication facilities that can achieve the best features in both terrestrial and satellite systems. Relative to the terrestrial cellular base station (BS), the HAP has a wide coverage area and is more flexible and non-polluting. Furthermore, when compared with satellite communication technologies, it consumes far less energy and has low propagation, which means greater QoS for real-time

users [3]. Massive MIMO is a technology used on HAPs that can improve energy efficiency and data rates by deploying a massive number of antennas, allowing multiple users to be served with the same time and frequency resources [4].

Massive MIMO technology allows high data rate transmissions by using the high number of antennas on the HAPs. Moreover, the enormous number of antennas in an array can provide sufficient gain by precoding, which can overcome the free space path loss [5]. However, in conventional fully digital (CFD) MIMO systems, each antenna requires a dedicated energy-intensive RF chain, which consumes a significant amount of energy (approximately 250 mW per RF chain). The energy consumption of CFD systems is too high due to the massive number of RF chains [6]. This allows researchers to consider hybrid (analog-to-digital) MIMO systems, which significantly reduce the number of RF chains by switching some operations to an analog domain [7].

A fully digital precoding technique demands a precise radio frequency (RF) chain consisting of a digital-to-analog converter (DAC), mixer, filter, and power amplifier for each antenna. When a large number of transmitting antennas is employed in the massive MIMO scenario, this results in prohibitively high hardware costs as well as significant energy consumption [8]. To solve this issue, recently, finite-resolution PS schemes have been developed. In this scheme, finite-resolution PSs are used directly instead of high-resolution phase shifters. This can lower the energy consumption of a PS network without loss of performance, but it still demands a large number of PSs, each of which consumes a significant amount of energy [9].The other scheme is to use the switch network instead of the PS network [10]. This can considerably minimize hardware costs and energy utilization, but it has a noticeable performance loss.

Few studies have specifically addressed the shortcomings of power consumption, SE, and achievable sum rates for HAP networks, in contrast to the extensive research that has been undertaken in the spectrum sharing and theoretical analysis of HAP [11–14].

Due to the enormous amount of power consumed by base stations (BSs), energy efficiency (EE) has been viewed as an essential criterion for the development of future communication networks, both from an economic and environmental point of view. In this connection, the authors in [15] jointly optimized the transmission beamforming and covariance matrix in a MISO system in order to maximize the equivalent efficiency (EE). The authors of [16,17] addressed the EE maximization problem for terrestrial-aerial networks and proposed two array signal-processing approaches based on Dinkelbach's transformation in order to achieve suboptimal solutions. However, fully connected HP requires an extremely large number of active antennas and RF chains, which causes the existing techniques, such as those in [16,18,19], to have an extremely high level of hardware power consumption, which in turn results in a low level of system EE. In [20], the authors established beamforming techniques aimed at the mmWave HAP system. These algorithms were built for planar arrays that had thousands of antenna elements. The work in [21] presents HP for HAP massive MIMO systems in order to obtain the RF and the baseband precoder with limited RF chains. The authors applied duality to exploit the relation between the RF precoder and the statistical CSI, which is complicated to tackle. In [22], the authors proposed two stages of outer precoding design with the assumption of a zero-precoding (ZF) inner pre-beamformer and iterative algorithm to achieve the sum rate result for HAP. The authors of [23] used NOMA-based HAP communications and multiple antennas to satisfy the connectivity, dependability, and high data rate needs of 5G-and-beyond applications. Furthermore, a user selection and correlation-based user corresponding method for a NOMA-based multi-user HAPS system were proposed. In [24,25], the authors designed an outer beamformer to reduce the dimensional statistical eigen mode of the users and user grouping algorithm for HAP massive MIMO systems. The work in [26,27] proposed HAP to perform the beamforming technique. For this, the authors realized the interference alignment method for achieving the maximum sum rate of HAPs, respectively. In [28], the authors realized a decreased channel state information (CSI) overhead in a sub-connected RF precoding scheme, but this is incompatible with HAP massive MIMO systems. In [29],

the initial RF precoder selection from a discrete codebook and the proposed algorithm iteration were utilized together to develop the RF precoder, avoiding an exhaustive search while maintaining a high level of complexity. The published literature did not focus on reducing the complexity of the architecture or energy consumption of the system, while in our proposed machine learning technique, we use limited RF chains and sub-connected HP with low-bit PSs for HAP massive MIMO systems, which reduces the power consumption and complexity and improves the overall sum rate, energy, and spectral efficiency (SE).

In the proposed work, we examined energy-efficient HP sub-connected one- and two-bit PSs for HAP massive MIMO systems, and our main contributions are the following:

- We investigate the energy consumption analysis to unveil the fact that the HPs based on a sub-connected low-bit PS architecture is substantially lower than that consumed by HR-PS-based HP. Moreover, utilizing one-bit PSs results in a slight and constant array gain loss.
- We propose 1- and 2-bit sub-connected PSs for an HAP massive MIMO system with significantly reduced hardware cost, complexity, and energy consumption in the Rician fading channel. The sub-connected HP design is expected to be easier to deploy and be more energy efficient. The sub-connected architecture is more practicable for antenna deployment due to its lower cost and lower hardware complexity.
- We propose ACE-based optimization with low-bit PSs to optimize the achievable sum rate, EE, and SE. First, our scheme randomly generates several candidate elements according to the probability distribution (PD) in HP, and then it weights them according to their sum rates, thereby improving the HP elements' PD by decreasing the cross-entropy. By repeating this process, we ultimately generate an HP with a sufficiently high probability close to the optimized level.
- We further examine the simulation results to show the fact that the HPs based on a sub-connected low-bit PS architecture can achieve near-optimum EE and sum rates compared with the traditional schemes.

The rest of this paper is arranged accordingly. Section 2 is about the energy consumption analysis of different hybrid precoding schemes. Section 3 is a brief description of the channel and system model, presenting ideas and steps for algorithms, ACE-based HPs with M-bit PSs, and complexity analysis. The experiment and discussion are in Section 4. The conclusions are in Section 5.

Notations: Lowercase and boldface $\mathbf{x}$ is used to denote the vector, and uppercase and boldface $\mathbf{X}$ is used to denote the matrix, while letters without boldface denote scalars. $(.)^T$ denotes a transpose, $(.)^{-1}$ denotes an inversion, $|.|$ denotes an absolute operator, $(.)^H$ denotes a conjugate transpose, $\|.\|_F$ denotes the Frobenius norm, $(.)^+$ denotes a pseudo inversion, $\otimes$ denotes the Kronecker product, and $\mathbf{I}_N$ denotes an $N \times N$ identity matrix.

2. Energy Consumption Analysis of Different Hybrid Precoding Schemes

Here, we discuss a fully connected, high-resolution phase shifter (e.g., 4 bits) hybrid precoding-based architecture in which every RF chain is connected to each antenna through the network. The high-resolution (HR) PS-based hybrid precoding energy consumption can be represented as follows:

$$P_{HR-PSs} = P + N_{RF}P_{RF} + NN_{RF}P_{HR-PS} + P_B \tag{1}$$

In Equation (1), P represents the total transmission power, P_{RF} is the power consumed by the RF chain, P_{HR-PS} depicts the energy consumed by the PSs, P_B represents the baseband power consumption, N shows the number of PSs, and N_{RF} represents the number of RF chains. The energy consumed by the HR-PSs is (P_{HR-PS} = 40 mW) for the 4-bit phase shifters. The HR-PS-based HP architecture can attain the achievable sum-rate, but it requires a large number of PSs. As stated in [30], the power consumption by HR-PSs is quite high. Thus, to overcome this problem, a switch-based HP was introduced in [7], where instead of HR-PSs, switches were used, which could also decrease the hardware cost.

Nevertheless, this switch-based solution cannot actually obtain the array gain of mmWave massive MIMO systems. We describe the system in [7] as follows:

$$P_{Sw-PSs} = P + N_{RF}P_{RF} + N_{RF}P_{Sw} + P_B \tag{2}$$

where P_{Sw} is the power consumed by the switches, which is much lower than the HR-PSs (e.g., P_{Sw} = 5 mW) [31]. However, this design cannot achieve the array gain since only the N_{RF} antennas are active simultaneously, resulting in sum rate performance degradation.

In a sub-connected one-bit PS-based HP architecture, in which each RF chain is attached to the subantennas of an array with N/N_{RF}, the power consumption is much lower than in a fully connected architecture [7], and it provides the better trade-off between the two precoding schemes. The energy consumed by a sub-connected HP architecture can be express as

$$P_{SubC-PSs} = P + N_{RF}P_{RF} + NP_{SubC} + P_B \tag{3}$$

It is noted that energy consumed by an HP architecture sub-connected with one or two bits is low (P_{SubC} = 5 mW). Therefore, compared with HR-PSs, the sub-connected PS energy consumption is too low. Aside from that, the proposed sub-connected PS HP architecture is able to use all antennas to achieve the optimal array gain compared with SW-based HP [32]. Compared with the fullly connected HP architecture, the sub connected HP architecture with one- or two-bit PSs has a significantly lower number of phase shifters from $N_t \times N_t^{RF}$ to N_t, which will have more benefits and will excite the PSs. It can save energy and compensate the insertion loss of PSs. In addition, it also has less complexity due to its simplicity in its architecture and configurations.

3. Channel and System Model

We adopted a multi-user HAP massive MIMO system where an HAP was equipped with a uniform planner array (UPA) with C number of antennas in each column, while the number of antennas in each row was $N = C \times A$, as shown in Figure 1, and each RF chain was connected to a subset of the antenna serving K single-antenna users, as shown in Figure 2. The received signal at the kth user can be expressed as follows:

$$\mathbf{y} = \mathbf{H}\mathbf{F_A}\mathbf{F_D}\mathbf{s} + \mathbf{n} \tag{4}$$

where $\mathbf{s}$ denotes the transmission signal of a size $K \times 1$, while $\mathbf{F_A}$ is of a size $N \times N_{RF}$ and $\mathbf{F_D}$ is of a size $N_{RF} \times K$ for the analog and digital precoder, respectively. In addition, $\mathbf{n}$ represents the additive white Gaussian noise vector with a distribution $\mathcal{CN}(0, \mathbf{I}_K)$. $\mathbf{H} = [\mathbf{h_1}, \mathbf{h_2}, \ldots \mathbf{h_k}]$ denotes the overall downlink channel matrix of a size $K \times N$, where $\mathbf{h_k} \in \mathbb{C}^{N \times 1}$ is the channel vector for the kth user, which can be expressed as

$$\mathbf{h_K} = \sqrt{\alpha}\left(\sqrt{\frac{K_{r,k}}{K_{r,k}+1}}\mathbf{h_{LK}} + \sqrt{\frac{K_{r,k}}{K_{r,k}+1}}\mathbf{h_{NLK}}\right) \tag{5}$$

where K_r represents the Rician factor, $\alpha = (4\pi r_k/\lambda)^{-2}$ is the large scaling factor for the kth user, r_k represents the distance between the HAP and the kth user, as shown in Figure 1, and λ is the carrier wavelength, while $\mathbf{h_{LK}}$ and $\mathbf{h_{NLK}}$ are the line-of-sight (LOS) components and non-line-of-sight (NLOS) components, respectively, which can be expressed as [33]

$$\mathbf{h_{LK}} = \mathbf{a}(\theta_k, \phi_k) \otimes \mathbf{x}(\theta_k, \phi_k) \tag{6}$$

$$\mathbf{h_{NLK}} = \sqrt{\hat{\mathbf{W}}_k}[w_{1k}, w_{2k}, \ldots w_{Nk}]^T \tag{7}$$

where $\mathbf{a}(\theta_k, \phi_k) = [1, e^{(j2\pi d_h), \ldots} \exp(2\pi(N-1)d_h)]^T$, $\mathbf{x}(\theta_k, \phi) = [1, e^{(j2\pi d_v), \ldots} \exp(2\pi(N-1)d_v)]^T$, the angles $\theta_k \in [-\pi, \pi]$ and $\phi_k \in [0, \pi/2]$ are the angles of departure (AoDs), d is the

distance between two adjacent antenna elements, and $\hat{\mathbf{W}}_{\mathbf{k}} \in \mathbf{C}^{N \times N}$ is the correlation matrix of the user K, which can be represented as follows:

$$[\hat{\mathbf{W}}_{\mathbf{k}}]_{a,b} = \int\limits_{0}^{\pi/2} \int\limits_{-\pi}^{\pi} f(\theta) f(\phi) \mathrm{e}^{(j\frac{2\pi}{\lambda}(d_1 - d_2))} d\theta d\phi \tag{8}$$

where $d_2 = (a-b)d_d \cos(\phi)\cos(\theta)$, $d_1 = (a-b)d_v \cos(\phi)\sin(\theta)$, $f(\phi) = e^{(-\sqrt{2}|\phi - \phi_0|/\sigma)}$, in which σ and ϕ_0 are the mean AoDs, $f(\theta) = e^{\kappa \cos(\theta - \mu)}/2\pi I_0(\kappa)$, I_0 is the zero-order Bessel function of the first kind, $\mu = (-\pi, \pi)$ is the mean angle of departure (AoD) of user K, and κ is the angular spread.
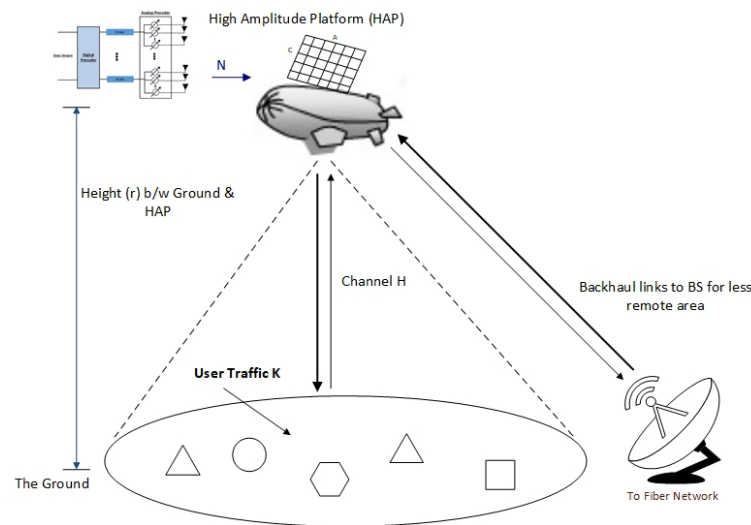
Figure 1. HAP massive MIMO system with user K.
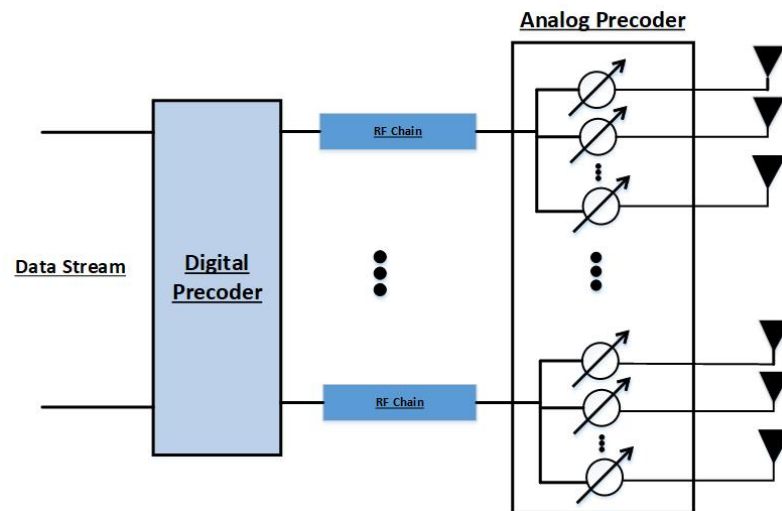
Figure 2. Sub-connected hybrid precoding architecture.

Furthermore, we need to explain the hardware constraints imposed by the proposed low-bit-based sub-connected HP, which differ from those imposed by traditional architectures. The first constraint is that the analog precoder $\mathbf{F_A}$ must be a block diagonal matrix rather than a full matrix:

$$\mathbf{F_A} = \begin{pmatrix} \mathbf{f_1} & \cdots & \mathbf{0} \\ \vdots & \ddots & \vdots \\ \mathbf{0} & \cdots & \mathbf{f_n} \end{pmatrix} \tag{9}$$

where the analog weighting vector for the nth sub antenna array is $\mathbf{f_n}$ with a size $N \times 1$. These components have the same amplitude but different phases. All N nonzero elements $\mathbf{F_A}$ should belong to

$$\frac{1}{\sqrt{N}}[-1,+1] \tag{10}$$

Our main objective is to develop an efficient hybrid precoders $\mathbf{F_A^{opt}}$ and $\mathbf{F_D^{opt}}$ to maximize the sum rate R, which can be written as

$$
\begin{aligned}
&\left(\mathbf{F_A^{opt}}, \{\mathbf{F_D^{opt}}\right) = \arg\max \mathbf{R}_{(sum)} \\
&\mathbf{F_A^{opt}}, \mathbf{F_D^{opt}} \\
&\text{s.t. } \mathbf{F_A^{opt}} \in \Re
\end{aligned}
$$

$$\sum_{m=1}^{M} \left\| \mathbf{F_A^{opt}}, \mathbf{F_D^{opt}} \right\|_F^2 = \rho \tag{11}$$

where $\Re$ represents the set of all possible analog precoders that satisfy the constrains in Equations (9) and (10). The sum rate can be expressed as

$$R_k = \sum_{k=1}^{K} \log_2(1 + \eta_k) \tag{12}$$

where η_k represents the signal-to-interference-plus-noise ratio (SINR) for the kth user, which can be expressed as follows:

$$\eta_k = \frac{\left| \mathbf{h_k^H} \mathbf{F_A} \mathbf{b_D^k} \right|^2}{\sum_{\bar{k} \neq k}^{K} \left| \mathbf{h_k^H} \mathbf{F_A} \mathbf{b_D^{\bar{k}}} \right|^2 + K\sigma^2} \tag{13}$$

Here, σ^2 represents the noise power, and $\mathbf{b_D^k}[m]$ represents the kth column of $\mathbf{F_D}$. It is worth mentioning that the constraints in Equations (9) and (10) on the analog precoder $\mathbf{F_A}$ are non-convex. This makes Equation (12) incredibly difficult to solve. The number of possible $\mathbf{F_A}$ values is finite, since all nonzero elements belong to the constraint in Equation (10). In order to tackle this challenging problem, we propose a machine learning (ML) adaptive cross-entropy optimization (ACE) with a low-bit, PS-based HP scheme.

3.1. Proposed ACE-Based Hybrid Precoding

To overcome the non-convex problem mentioned in Equations (9) and (10), we first decouple the joint design of the analog and digital precoders. As all of the analog precoder's N nonzero elements belong to Equation (10), the number of possibilities $\mathbf{F_A}$ is finite. As a result, we can consider the problem in Equation (11) to be a non-coherent combining problem. We can select an $\mathbf{F_A}$ candidate first and compute the optimal $\mathbf{F_D}$ with an efficient channel matrix $\mathbf{HF_A}$ without non-convex constraints. After searching for all possible $\mathbf{F_A}$ values, we can find the optimum analog precoder $\mathbf{F_A^{opt}}$ and digital precoder $\mathbf{F_D^{opt}}$. Unfortunately, such an exhaustive search involves filtering through all possible 2^N combinations, requiring excessively high complexity as the number of antennas N required is typically higher in massive MIMO systems, which in this case is N = 64, $2^{64} = 1.8 \times 10^{19}$. To tackle this challenging problem, we proposed an ACE algorithm with a one- or two-bit PS-based HP scheme, which is the advanced version of the CE algorithm [34]. In the CE algorithm, all elite contributions are treated as equal. Logically, when updating the PD, the elite contributions with better values should be more important. Therefore, if we can weight the elites as per their objective values, then we can expect better results. In ACE, multiple candidates' HP schemes are randomly generated based on the PD of the element in the HP. Then, they are weighted according to their sum rates for the calculated candidate HP. To enhance the probability distribution (PD) of an element $\mathbf{F_A}$, we reduce the CE between the two PDs.

We formulated the non-zero elements in $\mathbf{F_A}$ as an $N \times 1$ vector at the beginning, which can be expressed as $\mathbf{f} = \left[(\mathbf{f_1^A})^T, (\mathbf{f_2^A})^T, \dots (\mathbf{f_{NA}^A})^T \right]^T$, and the probability function $\mathbf{q} = [q_1, q_2, q_3, \dots q_N]^T$ as the $N \times 1$ vector. The probability is denoted by $0 \le q_n \le 1$, where $f_n = \frac{1}{\sqrt{N}} f_n$ is the nth element of $\mathbf{f}$. First, we initialized $\mathbf{q}^{(0)}$ as $\mathbf{q}^{(0)} = \frac{1}{2} \times 1_{N \times 1}$ after setting the initial values of the parameters, namely the parameter for the ACE-based HP with sub-connected low-bit PSs. The updated method has the steps presented below.

In step 3, we produce the Z candidate analog precoder $\{\mathbf{F_A^z}\}_{z=1}^Z$, which depends upon the probability distribution function $\Xi(\Re; q^{(i)})$, and in step 4, we calculate the digital precoding $\mathbf{F_D}$ based on the efficient channel $(\mathbf{H}_{eq}^z)^H = \mathbf{H}\{\mathbf{F_A^{opt}}\}$. We employed a zero-forcing digital precoding scheme with low complexity and near-optimal performance in this paper, which can be expressed as

$$\mathbf{G}^z = (\mathbf{H}_{eq}^z)^H \left(\mathbf{H}_{eq}^z (\mathbf{H}_{eq}^z)^H \right)^{-1} \tag{14}$$

$$\mathbf{F_D^z} = \beta^z \mathbf{G}^z \tag{15}$$

where $\beta^z = \frac{\sqrt{\rho}}{\|\mathbf{F_A^z G}^z\|_F}$ represents the power-normalized factor.

In step 5, we calculate the achievable sum rate by putting $\mathbf{F_A^z}$ and $\mathbf{F_D^z}$ in Equation (12). The achievable sum rates will be sorted in descending order in step 6. In step 7, the elite Z_{elite} values can be obtained with the highest sum rate. These candidates are utilized to update the probability distribution $\mathbf{q}^{i+1}$ and minimize the CE, which is equivalent to [34]

$$\mathbf{q}^{i+1} = \arg\max \frac{1}{Z} \sum_{z=1}^{Z_{elite}} \ln \Xi \left(\Re_A^{[z]} \mathbf{q}^{(i)} \right) \tag{16}$$

where $\Xi \left(\Re_A^{[z]} \mathbf{q}^{(i)} \right)$ is the probability to output $\mathbf{F_A^z}$ as stated in Equation (16). All elites have the same effects, and this leads to decreased performance. In order to fix this problem, we propose adaptively weighting the elites depending upon their sum rates. Thus, an auxiliary parameter U, which denotes the average of all sum rates, is introduced.

$$U = \frac{1}{Z_{elite}} \sum_{z=1}^{Z_{elite}} R(\mathbf{F_A^{[z]}}) \tag{17}$$

The weight w_z of the elite $\mathbf{F_A^z}$ can be calculated in step 8 based on $\{w\}_{z=1}^{Z_{elite}}$, and Equation (15) can be modified to become

$$\mathbf{q}^{(i+1)} = \arg\max \frac{1}{Z} \sum_{z=1}^{Z_{elite}} w_z \ln \Xi \left(\Re_A^{[z]} \mathbf{q}^{(i)} \right) \tag{18}$$

where $\Xi \left(\Re_A^{[z]} \mathbf{q}^{(i)} \right)$ is the probability to calculate the $\mathbf{F_A^z}$. Notice that $\Xi \left(\Re_A^{[z]} \mathbf{q}^{(i)} \right) = \Xi \left(\mathbf{f}^{[z]}; \mathbf{q}^{(i)} \right)$, the nth element $f_n^{(z)}$ of $\mathbf{f}^{[z]}$, is the Bernoulli random variable, where $f_n^{(z)} = \frac{1}{\sqrt{N}}$ has a probability $q_n^{(i)}$, and similarly, $f_n^{(z)} = -\frac{1}{\sqrt{N}}$ has a probability $1 - q_n^{(i)}$. Thus, we have

$$\Xi \left(\Re_A^{[z]} \mathbf{q}^{(i)} \right) = \prod_n^N (q_n^{(i)})^{\frac{1}{2}(1+\sqrt{N} f_n^{(z)})} (1 - q_n^{(i)})^{\frac{1}{2}(1+\sqrt{N} f_n^{(z)})} \tag{19}$$

By putting Equation (19) into Equation (18), the first-order derivatives based on $q_n^{(i)}$ from Equation (18) is given as follows:

$$\frac{1}{Z} \sum_{z=1}^Z w_z \left(\frac{1 + \sqrt{N} f_n^{(z)}}{2 q_n^i} - \frac{1 + \sqrt{N} f_n^{(z)}}{2(1 - q_n^i)} \right) \tag{20}$$

For Equation (20), when set to zero, $1 - q_n^{(i)}$ is updated in step 9 as follows:

$$q_n^{(i+1)} = \frac{\sum\limits_{z=0}^{Z_{elite}} w_z \left(\sqrt{N} f_n^{(z)} + 1 \right)}{2 \sum\limits_{z=1}^{Z_{elite}} w_z} \tag{21}$$

We can further simplify Equation (21) to avoid the local optimum:

$$q_n^{(i+1)} = \Omega^{i+1} \times q_n^{(i+1)} + (1 - \Omega^{i+1}) \times q_n^{(i)} \tag{22}$$

where Ω^{i+1} in iteration $(i+1)$ is a smooth size for the step. We used steps 3–10 for the pre-defined iteration. Finally, the optimal analog $\mathbf{F_A^{opt}}$ and digital precoding $\mathbf{F_D^{opt}}$ are obtained.

3.2. ACE-Based Hybrid Precoding with M-Bit PS

We present a more general case (i.e., m-bit PSs) for the proposed ACE-based HP. We first generated the parametric sample distribution, which produced the applicant alternatives for the next iterations. The simple method of producing a random sample $\hat{\mathbf{b}} = \{\hat{\mathbf{b}}\}_{n=1}^N$ is to draw independently from $\{\hat{b}_1, \hat{b}_2, \ldots \hat{b}_N\}$. Here, each sample belongs to a discrete distribution $\{\mathbf{q}_{m,n}^{(i)}\}$, and the mth quantized process of a set M is chosen to be $\hat{b}_n$. The elite candidates should then change the potential to minimize the CE:

$$\mathbf{q}_{m,n}^{(i+1)} = \arg \max_{q(i)} \frac{1}{Z} w_z \sum_{z=1}^{Z_{elite}} \ln \Xi \left(\Re_A^{[z]} \mathbf{q}_{m,n}^{(i)} \right) \tag{23}$$

where $\Xi \left(\Re_A^{[z]} \mathbf{q}_{m,n}^{(i)} \right)$ is given by

$$\Xi \left(\Re_A^{[z]} \mathbf{q}_{m,n}^{(i)} \right) = \prod_n^N \sum_{m=1}^M w_z (q_{m,n}^{(i)}) \mathbf{1}_{\{\hat{\mathbf{a}}^{(z)} \in \Re_{m,n}\}} \tag{24}$$

The indicator function is $\mathbf{1}_{\{.\}}$ if the statement is valid (i.e., = 1); otherwise, $\mathbf{1}_{\{.\}} = 0$. In addition, $\Re_{m,n} = \hat{\mathbf{b}} \in M^N : \hat{b}_n = \frac{2\pi m}{|M|}$, in which $M = \left\{ \frac{2\pi m}{2^M} (z = 1, \ldots, 2^M) \right\}$ refers to the set containing all possible analog precoders which satisfy the given constraint in Equation (9). Here, it is given that a single PS can be allocated to only one quantized process. The sum of every constrained probability is equal to one, and we implement the Lagrange multiplier to fulfill the constraints:

$$\mathbf{q}_{m,n}^{(i+1)} = \arg \max_{q(i)} \frac{1}{Z} w_z \sum_{z=1}^{Z_{elite}} \ln \Xi \left(\Re_A^{[z]} \mathbf{q}_{m,n}^{(i)} \right) + \sum_{n=1}^N L_n \left(\sum_{m=1}^M \mathbf{q}_{m,n}^{(i)} - 1 \right) \tag{25}$$

When we take the first derivative of Equation (25) with respect to the probability $\mathbf{q}_{m,n}^{(i)}$ and then set the outcome to zero, we obtain the following result:

$$\frac{1}{Z} \sum_{z=1}^{Z_{elite}} \mathbf{1}\{\hat{\mathbf{a}}^{(z)} \in \Re_{m,n}\} + L_n \mathbf{q}_{m,n}^{(i)} = 0 \tag{26}$$

Finally, we add Equation (26) for $m = 1, 2, \ldots, M$, and we modify the probability as given below:

$$\mathbf{q}_{m,n}^{(i+1)} = \frac{\sum\limits_{z=1}^{Z_{elite}} w_z \{\hat{\mathbf{a}}^{(z)} \in \Re_{m,n}}{\sum_{z=1}^{Z_{elite}} w_z} \tag{27}$$

3.3. Complexity Analysis

According to Algorithm 1, the difficulty of the proposed ACE-based HP sub-connected low-resolution bit PS scheme initiates steps 4, 5, and 9. As in step 4, the effective channel

matrices $\left\{\mathbf{H}_{\text{eq}}^{Z}\right\}_{z=1}^{Z}$ for each candidate solution Z, as well as the related digital precoder $\left\{\mathbf{F}_{\text{D}}^{z}\right\}_{z=1}^{Z}$, must be calculated as in Equations (15) and (16). As a result, this component has a complexity of $Z(NZK^2)$. In step 5, the sum rate for each candidate solution is computed. Here, we employ the traditional ZF precoder, which reduces the SINR of each user for each candidate to $\gamma^z = (\beta^z/\sigma)^2$. According to Equation (22), step 9 is the updating step of $\mathbf{q}_n^{(i+1)}$, which composes the complexity of $Z(NZ_{\text{elite}})$. After I iterations, the overall computational cost of the proposed ACE-based HP sub-connected low-resolution bit system PS is $Z(ZINK^2)$. Meanwhile, I and Z are not essentially so big. This enables the complexity of the ACE-based HP sub-connected low-resolution bit PS to be reasonable and comparable to some current methods.

Algorithm 1 ACE-based hybrid precoding with sub-connected phase shifters (PSs)

Input:
Rician Channel-Matrix H, Iterations I, Candidates Z, Elites Z_{Elite}, Smoothing Step size Ω

Output:
Analog Precoder $\mathbf{F_A^{opt}}$, Digital Precoder $\mathbf{F_D^{opt}}$

1.　initialization i = 0,$\mathbf{p} = 1/2 \times \mathbf{1}_{N\times 1}$
2.　**for** $iteration = 1, 2, \ldots$
3.　Generate Z candidates randomly as $\{\mathbf{F_A^{opt}}\}_{z=1}^{Z}$ based on $\Xi(\Re; q^{(i)})$
4.　Calculate Z digital precoder $\{\mathbf{F_D^{opt}}\}_{z=1}^{S}$ based on effective channel by (15)
5.　Calculate the sum-rate $\mathbf{R}\{\mathbf{F_A^{opt}}\}_{z=1}^{Z}$ by (12)
6.　Sorting $\mathbf{R}\{\mathbf{F_A^{opt}}\}_{z=1}^{Z}$ in descending order as $\mathbf{R}(\mathbf{F_A^{[1]}} \geq \mathbf{F_A^{[2]}} \geq, \ldots, \mathbf{F_A^{[Z]}})$
7.　Select elite as $\mathbf{F_A^{[1]}}, \mathbf{F_A^{[2]}}, \ldots, \mathbf{F_A^{[Z_{Elite}]}}$
8.　Calculate weight for each elite $\mathbf{F_A^{[S]}}$ according to their sum-rate
9.　Update the probability $\mathbf{q}^{(i+1)}$ according to weight and $\{\mathbf{F_A^{opt[z]}}\}_{z=1}^{Z_{Elite}}$
10.　**end for**

---

4. Experiment and Discussion

In this section, we will discuss the effectiveness of the ACE-based optimization that was proposed with low-bit PSs in terms of the achievable sum rate, EE, and SE. The following are the primary simulation parameters. We used the assumption that the users were dispersed in a 20-km radius under the HAP circle, and the height of the HAP was 20 km. It operated at a frequency of 2.4 gigahertz. The number of transmitting antennas $C = A = 10$, the transmitting power P was set to 20 dB, and we set the bandwidth to 10 MHz. The Rician factor K_r =10, and the transmitting antenna array was a UPA with antenna spacing $d = 2\lambda$. The number of RF chains was four. Furthermore, the number of candidate solutions, the number of elite candidates, and the number of iterations were set to $Z = 200$, $Z_{elite} = 40$, and $I = 20$, respectively.

Figure 3 presents that the proposed ACE sub-connected low-bit PS-based HP obtained a higher sum rate than the technique that is currently being used for HAP massive MIMO systems. For the ACE-Algorithm 1, the values were the same as above. The zero-forcing (ZF) precoding system is designed for use with the fully connected PS architecture, whereas the hybrid precoding system for conventional analog selection (AS) is designed for the switch-based architecture. When compared with CE, the ACE-based HP method has only one more step, but this step has a minimally increased level of complexity. The proposed ACE algorithm is, therefore, more effective. In Figure 3, we can see that the sum rate of the proposed ACE-based low-bit PSs was significantly higher than that of traditional AS-based HP and CE-based HP, and the difference between the ZF precoding and ACE-based HP remained constant. Nevertheless, the gap can be closed if the PSs continue to increase in terms of their resolution.
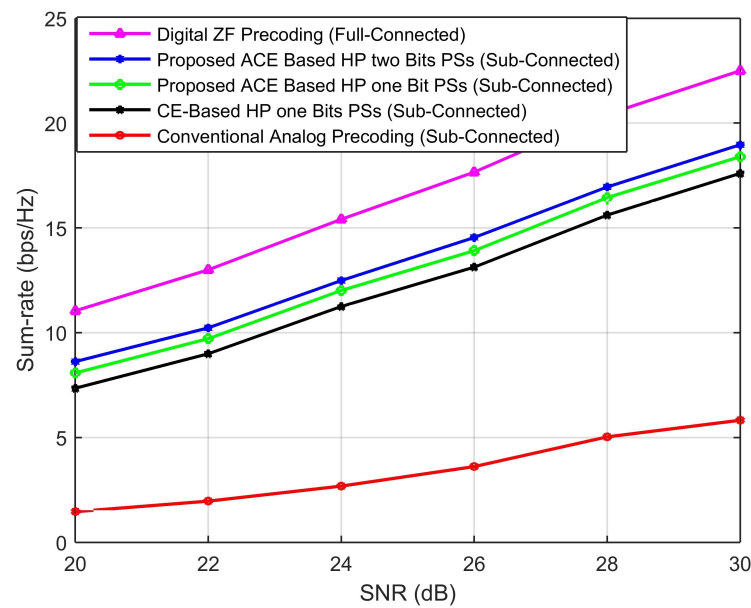
Figure 3. Sum-rate of ACE-based method with sub-connected PSs when C = A = 10 and users and RF chains are 4.

Figure 4 compares the sum rates that can be achieved by the proposed ACE-based HP with sub-connected low-bit PSs to the sum rates that can be achieved by the existing solutions for the HAP massive MIMO system. We used 8 for the number of RF chains and 8 for the number of users K, while the number of antennas C = A = 12. The remaining parameters are the same ones that were discussed above. It is evident from this that the proposed solution with sub-connected low-bit PSs was capable of achieving a significantly higher sum rate than the conventional HP, CEO-based HP with one-bit PSs, and fully connected ZF-based HP gap. In addition, a noticeable performance gap may be seen between the proposed solutions, which used 1-bit and 2-bit PSs, and the HR-based full-connected HP, which used 4-bit PSs. However, this gap could be narrowed by increasing the resolution of the PSs.
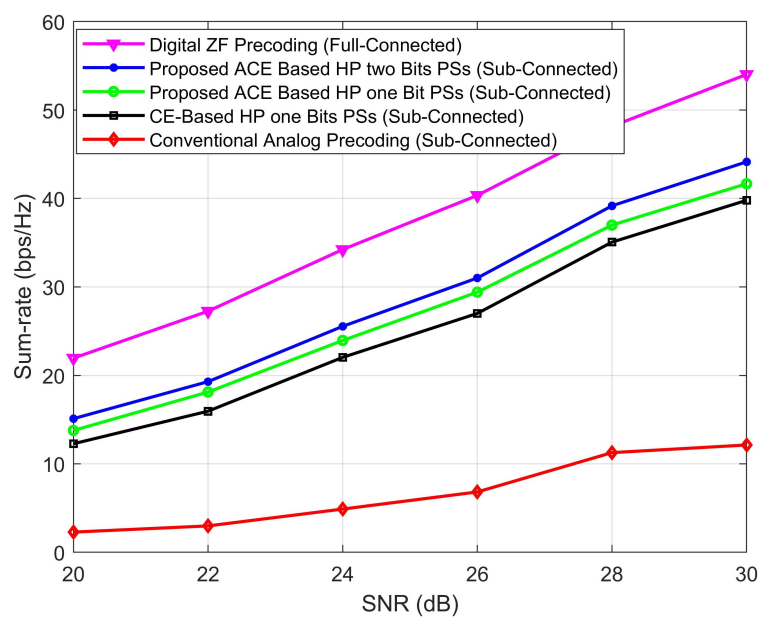
Figure 4. Sum rates of ACE-based method with sub-connected PSs when C = A = 12 and user count and RF chain are 8.

Figure 5 presents the energy efficiency attained by the proposed ACE-based HP with sub-connected PSs and some existing HP schemes mentioned above. The number of RF chains was equal to the user count K, and it varied from 1 to 32, while the other parameters were similar to those in Figure 2. In accordance with [35], the energy efficiency was calculated as the ratio of the sum rate to the total power consumption:

$$EE = \frac{R_{sum}}{p_{total}} (bps/Hz/W) \tag{28}$$
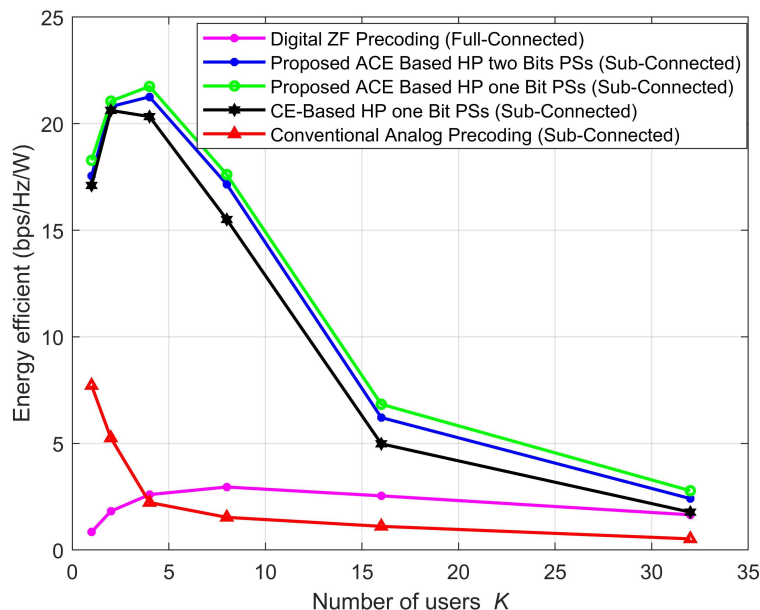
Figure 5. Energy efficiency of ACE-based method with sub-connected PSs (when C = A = 10), where SNR = 30.

The practical values for power consumption are as follows. The energy consumed by the sub-connected architecture where p = 0.03 W for the baseband power consumption is P_B = 0.2 W, the power consumed by the RF chain P_{RF} = 0.3 W, the one-bit PS power consumption P_{ps} = 0.005 W, and the typical valves of PS power consumption are 0.015 W, 0.045 W, 0.06 W, and 0.078 W for PSs of 3, 4, 5, and 6 bits, respectively [36,37]. Our proposed ACE-based HP scheme with sub-connected PSs attained a high value of energy efficiency when compared with other existing HPs, as mention above.

Figure 6 presents that the proposed ACE-based algorithm with low-bit PSs obtained improved SE in comparison with other sub-connected schemes, especially when the number of users was not extremely large. The number of users K could range from 1 to 32, and the RF chains had the same configuration as the users. The bandwidth was fixed at 10 MHz, and the other parameters were comparable to those shown in Figure 4. In addition, it can be seen that when K equaled eight, the proposed ACE with two-bit PSs had a greater spectral efficiency than other sub-connected schemes, with the exception of the ZF precoding fully connected method. The reason for this was that when the number of users and RF chains increased, the number of PSs also increased, leading to a sharp rise in the total number of PSs in systems that were PS-based. In practice, the utilization of PSs with high resolutions that need a significant amount of energy is not appropriate. The gap between the proposed algorithm and the ZF-based HP is constant behavior. This can be reduced by increasing the resolution of the PSs.
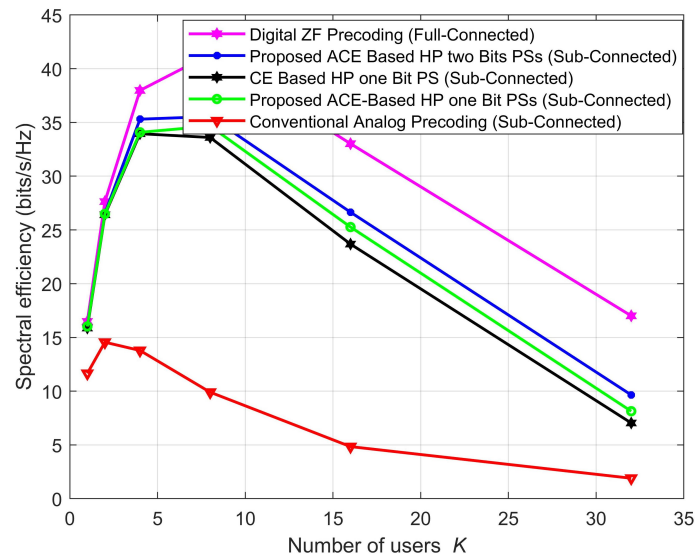
Figure 6. Spectral efficiency of ACE-based method with sub-connected PSs (when C = A = 10 and SNR = 30).

Finally, the impact of imperfect CSI was noticed in the proposed ACE-based HP, where $\hat{\mathbf{H}}$ represents the imperfect CSI as in [38]:

$$\hat{\mathbf{H}} = \varepsilon H + \sqrt{1 - \varepsilon^2}\mathbf{E} \tag{29}$$

where $\varepsilon \in [0, 1]$ represents the CSI accuracy, **H** is the original channel matrix, and **E** is the error matrix whose elements are distributed according to an independent and identically distributed distribution $\mathcal{CN}(0, 1)$. Figure 7 depicts the ACE-based HP sum rates for various CSI scenarios when $A = C = 10$ and N_{RF} and $K = 4$. We considered a number of flawed CSI cases with varying values in addition to a perfect CSI scenario. CSI accuracy is not a factor in the proposed ACE-based HP with one-bit PSs. The proposed scheme's sum rate, which was reached with a value of $\varepsilon = 0.8$, was quite close to the perfect CSI situation. Furthermore, even when the CSI accuracy was extremely low, as when *varepsilon* = 0.4, the ACE-based proposal could still achieve 80 percent of the sum rate.
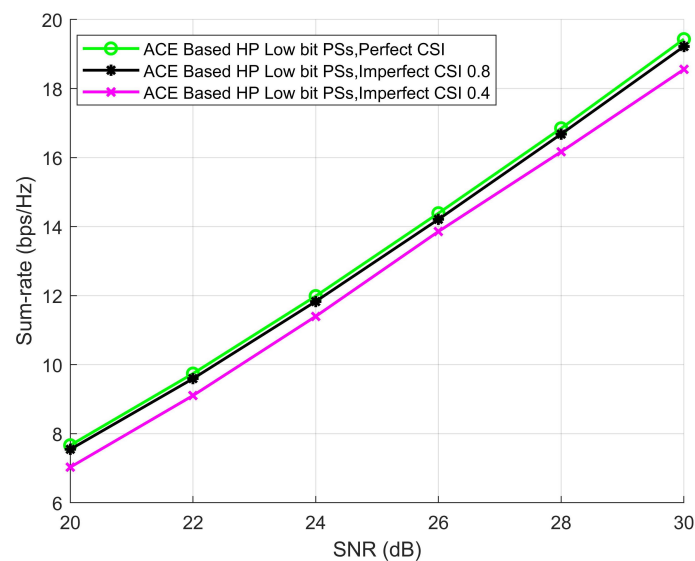
Figure 7. ACE-based HP with different CSI conditions (when C = A = 10 and users and RF chain = 4).

5. Conclusions

In this paper, we presented an EE design for HPs with a sub-connected low-bit PS HAP massive MIMO system. Initially, we focused on how to reduce power consumption without sacrificing performance. This energy utilization study showed that low-bit PS-based hybrid precoding consumes very little energy, and it also revealed that the array gain loss that is sustained by low-bit PSs is constrained and constant. Afterward, a low-complexity method that was based on ACE-based optimization with low-bit phase shifters was proposed in order to handle the sum rate maximization problem. The outcome of our simulation demonstrates that the proposed algorithm obtained a sufficiently high value for sum rate performance metrics as well as a higher value for energy efficiency compared with other algorithms.

Author Contributions: Study conception and design, preparation, data collection, analysis, and drafting, S.u.H.; conception, design, critical review for intellectual contents, and supervision, S.A.; data collection, analysis, and proofreading, T.M.; critical revision and drafting, N.A.K.; critical revision, U.M. All authors have read and agreed to the published version of the manuscript.

Data Availability Statement: Codes and other relevant data are available and will be uploaded to https://github.com/Hassanbangash12/HAP-Massive-MIMO-with-Limited-RF-Chains (accessed on 10 December 2022) after the acceptance and publication of the manuscript. Interested authors can access and download the simulation code from the given link.

Conflicts of Interest: The authors declare that they have no known competing financial interests or personal relationships that could have appeared to influence the work reported in this paper.

References

1. Mumtaz, S.; Rodriguez, J.; Dai, L. *MmWave Massive MIMO: A Paradigm for 5G*; Academic Press: Cambridge, MA, USA, 2016.
2. Tozer, T.; Grace, D. High-altitude platforms for wireless communications. *Electron. Commun. Eng. J.* **2001**, *13*, 127–137. [CrossRef]
3. Jia, Z.; Wu, Q.; Dong, C.; Yuen, C.; Han, Z. Hierarchical Aerial Computing for Internet of Things via Cooperation of HAPs and UAVs. *IEEE Internet Things J.* **2022**. [CrossRef]
4. Zhang, G.; Jiang, L.; Ji, P.; Zou, S.; He, C.; He, D. A Modified K-means User Grouping Design for HAP Massive MIMO Systems. In Proceedings of the 2021 International Conference on Networking and Network Applications (NaNA), Lijiang, China, 29 October–1 November 2021; pp. 288–292.
5. Liu, X.; Li, X.; Cao, S.; Deng, Q.; Ran, R.; Nguyen, K.; Tingrui, P. Hybrid precoding for massive mmWave MIMO systems. *IEEE Access* **2019**, *7*, 33577–33586. [CrossRef]
6. Huang, Y.; Liu, C.; Song, Y.; Yu, X. Near-optimal hybrid precoding for millimeter wave massive MIMO systems via cost-efficient Sub-connected structure. *IET Commun.* **2020**, *14*, 2340–2349. [CrossRef]
7. Gao, X.; Dai, L.; Han, S.; Chih-Lin, I.; Heath, R.W. Energy-efficient hybrid analog and digital precoding for mmWave MIMO systems with large antenna arrays. *IEEE J. Sel. Areas Commun.* **2016**, *34*, 998–1009. [CrossRef]
8. Alkhateeb, A.; Leus, G.; Heath, R.W. Limited feedback hybrid precoding for multi-user millimeter wave systems. *IEEE Trans. Wirel. Commun.* **2015**, *14*, 6481–6494. [CrossRef]
9. Lu, A.Y.; Chen, Y.F. Adaptive Hybrid Beamforming Schemes in Millimeter Wave MIMO Systems. In Proceedings of the 2021 IEEE International Symposium on Radio-Frequency Integration Technology (RFIT), Hualien, Taiwan, 25–27 August 2021; pp. 1–3.
10. Yu, J.; Lee, H.; Eom, C.; Lee, C. A Switch Network-Based Adaptive Sub-Connected Hybrid Precoding Architecture in Sub-THz Communications. In Proceedings of the 2021 36th International Technical Conference on Circuits/Systems, Computers and Communications (ITC-CSCC), Jeju, Korea, 27–30 June 2021; pp. 1–4.
11. Jo, S.; Yang, W.; Choi, H.K.; Noh, E.; Jo, H.S.; Park, J. Deep Q-Learning-Based Transmission Power Control of a High Altitude Platform Station with Spectrum Sharing. *Sensors* **2022**, *22*, 1630. [CrossRef]
12. Tashiro, K.; Hoshino, K.; Nagate, A. Nullforming-Based Precoder for Spectrum Sharing between HAPS and Terrestrial Mobile Networks. *IEEE Access* **2022**, *10*, 55675–55693. [CrossRef]
13. Sun, Z.; Qi, F.; Liu, L.; Xing, Y.; Xie, W. Energy-efficient Spectrum Sharing for 6G Ubiquitous IoT Networks Through Blockchain. *IEEE Internet Things J.* **2022**. [CrossRef]
14. Lin, Z.; Lin, M.; Wang, J.B.; De Cola, T.; Wang, J. Joint beamforming and power allocation for satellite-terrestrial integrated networks with non-orthogonal multiple access. *IEEE J. Sel. Top. Signal Process.* **2019**, *13*, 657–670. [CrossRef]

15. Lu, Y.; Xiong, K.; Fan, P.; Ding, Z.; Zhong, Z.; Letaief, K.B. Global energy efficiency in secure MISO SWIPT systems with non-linear power-splitting EH model. *IEEE J. Sel. Areas Commun.* **2018**, *37*, 216–232. [CrossRef]

16. Huang, Q.; Lin, M.; Wang, J.B.; Tsiftsis, T.A.; Wang, J. Energy efficient beamforming schemes for satellite-aerial-terrestrial networks. *IEEE Trans. Commun.* **2020**, *68*, 3863–3875. [CrossRef]

17. Niu, H.; Lin, Z.; Chu, Z.; Zhu, Z.; Xiao, P.; Nguyen, H.X.; Lee, I.; Al-Dhahir, N. Joint beamforming design for secure RIS-assisted IoT networks. *IEEE Internet Things J.* **2022**. [CrossRef]

18. Lin, Z.; Lin, M.; Champagne, B.; Zhu, W.P.; Al-Dhahir, N. Secrecy-energy efficient hybrid beamforming for satellite-terrestrial integrated networks. *IEEE Trans. Commun.* **2021**, *69*, 6345–6360. [CrossRef]

19. Lin, Z.; An, K.; Niu, H.; Hu, Y.; Chatzinotas, S.; Zheng, G.; Wang, J. SLNR-based secure energy efficient beamforming in multibeam satellite systems. *IEEE Trans. Aerosp. Electron. Syst.* **2022**. [CrossRef]

20. Srinivasan, M.; Gopi, S.; Kalyani, S.; Huang, X.; Hanzo, L. Airplane-aided integrated next-generation networking. *IEEE Trans. Veh. Technol.* **2021**, *70*, 9345–9354. [CrossRef]

21. Ji, P.; Jiang, L.; He, C.; He, D. Hybrid Precoding for HAP Massive MIMO Systems. In *Proceedings of the International Conference on Space Information Network*; Springer: Berlin/Heidelberg, Germany, 2019; pp. 255–263.

22. Zong, D.; Jiang, L.; He, C.; Ji, P.; He, D. Two-stage precoding design in Rician channel for HAP massive MIMO systems. In Proceedings of the 2019 22nd International Symposium on Wireless Personal Multimedia Communications (WPMC), Lisbon, Portugal, 24–27 November 2019; pp. 1–5.

23. Cumalı, İ.; Özbek, B.; Kurt, G.K.; Yanikomeroglu, H. User Selection and Codebook Design for NOMA-Based High Altitude Platform Station (HAPS) Communications. *IEEE Trans. Veh. Technol.* **2022**. [CrossRef]

24. Lian, Z.; Jiang, L.; He, C.; He, D. User grouping and beamforming for HAP massive MIMO systems based on statistical-eigenmode. *IEEE Wirel. Commun. Lett.* **2019**, *8*, 961–964. [CrossRef]

25. Ji, P.; Jiang, L.; He, C.; Lian, Z.; He, D. Energy-efficient beamforming for beamspace HAP-NOMA systems. *IEEE Commun. Lett.* **2020**, *25*, 1678–1681. [CrossRef]

26. Sudheesh, P.; Mozaffari, M.; Magarini, M.; Saad, W.; Muthuchidambaranathan, P. Sum-rate analysis for high altitude platform (HAP) drones with tethered balloon relay. *IEEE Commun. Lett.* **2017**, *22*, 1240–1243. [CrossRef]

27. He, Y.; Wang, D.; Huang, F.; Zhang, R.; Gu, X.; Pan, J. Downlink and Uplink Sum Rate Maximization for HAP-LAP Cooperated Networks. *IEEE Trans. Veh. Technol.* **2022**, *71*, 9516–9531. [CrossRef]

28. Teng, Y.; Wei, M.; Liu, A.; Lau, V.; Zhang, Y. Mixed-timescale per-group hybrid precoding for multiuser massive MIMO systems. *IEEE Signal Process. Lett.* **2018**, *25*, 675–679. [CrossRef]

29. Yu, H.; Qu, W.; Fu, Y.; Jiang, C.; Zhao, Y. A novel two-stage beam selection algorithm in mmWave hybrid beamforming system. *IEEE Commun. Lett.* **2019**, *23*, 1089–1092. [CrossRef]

30. El Ayach, O.; Rajagopal, S.; Abu-Surra, S.; Pi, Z.; Heath, R.W. Spatially sparse precoding in millimeter wave MIMO systems. *IEEE Trans. Wirel. Commun.* **2014**, *13*, 1499–1513. [CrossRef]

31. Méndez-Rial, R.; Rusu, C.; Alkhateeb, A.; González-Prelcic, N.; Heath, R.W. Channel estimation and hybrid combining for mmWave: Phase shifters or switches? In Proceedings of the 2015 Information Theory and Applications Workshop (ITA), San Diego, CA, USA, 1–6 February 2015; pp. 90–97.

32. Mir, T.; Siddiqi, Z.; Mir, U.; MacKenzie, R.; Hao, M. One-bit hybrid precoding for wideband millimeter-wave massive MIMO systems. In Proceedings of the 2019 IEEE 89th Vehicular Technology Conference (VTC2019-Spring), Kuala Lumpur, Malaysia, 28 April–1 May 2019; pp. 1–6.

33. Michailidis, E.T.; Kanatas, A.G. Three-dimensional HAP-MIMO channels: Modeling and analysis of space-time correlation. *IEEE Trans. Veh. Technol.* **2010**, *59*, 2232–2242. [CrossRef]

34. Rubinstein, R.Y.; Kroese, D.P. *The Cross-Entropy Method: A Unified Approach to Combinatorial Optimization, Monte-Carlo Simulation and Machine Learning*; Springer Science & Business Media: Berlin/Heidelberg, Germany, 2013.

35. Liu, Y.; Feng, Q.; Wu, Q.; Zhang, Y.; Jin, M.; Qiu, T. Energy-efficient hybrid precoding with low complexity for mmWave massive MIMO systems. *IEEE Access* **2019**, *7*, 95021–95032. [CrossRef]

36. Méndez-Rial, R.; Rusu, C.; González-Prelcic, N.; Alkhateeb, A.; Heath, R.W. Hybrid MIMO architectures for millimeter wave communications: Phase shifters or switches? *IEEE Access* **2016**, *4*, 247–267. [CrossRef]

37. Huang, C.; Alexandropoulos, G.C.; Zappone, A.; Debbah, M.; Yuen, C. Energy efficient multi-user MISO communication using low resolution large intelligent surfaces. In Proceedings of the 2018 IEEE Globecom Workshops (GC Wkshps), Abu Dhabi, United Arab Emirates, 9–13 December 2018; pp. 1–6.

38. Li, X.; Fang, J.; Li, H.; Wang, P. Millimeter wave channel estimation via exploiting joint sparse and low-rank structures. *IEEE Trans. Wirel. Commun.* **2017**, *17*, 1123–1133. [CrossRef]